Nanoscale Horizons

Controlling Exciton Transport in Monolayer $MoSe_2$ by Dielectric Screening

Journal:	*Nanoscale Horizons*
Manuscript ID	NH-COM-07-2019-000462.R1
Article Type:	Communication
Date Submitted by the Author:	06-Aug-2019

Complete List of Authors:	Hao, Shengcai; Beijing Jiaotong University Bellus, Matthew; University of Kansas He, Dawei; Beijing Jiaotong University Wang, Yongsheng; Beijing Jiaotong University Zhao, Hui; University of Kansas

Conceptual Insight

We introduce and demonstrate a concept of controlling exciton transport in 2D semiconductors by dielectric environment engineering. The concept of excitonic devices has been proposed for several decades; however, its implementation has been hindered by the lack of materials suitable for room-temperature operations. The recently discovered 2D semiconductors offer a promising system for such devices due to their stable excitonic states at room temperature. One challenge in excitonic devices is to control the transport of excitons, which are neutral quasiparticles and thus less responsive to an electric field. Using monolayer $MoSe_2$ as a model system, we demonstrate an approach to control exciton transport by altering the local dielectric environment with thin BN layers. The method is based on the fact that in 2D materials the Coulomb interaction between charged particles extends to the environment, which provides opportunities to control the electronic and optical properties of 2D materials by manipulating their surroundings. The results illustrate the feasibility of using dielectric engineering to control exciton transport and help understand the effects of dielectric environment on excitons and charge carriers.

Journal Name

ARTICLE TYPE

Cite this: DOI: 10.1039/xxxxxxxxxx

Controlling Exciton Transport in Monolayer $MoSe_2$ by Dielectric Screening†

Shengcai Hao,[a,b] Matthew Z. Bellus,[b] Dawei He,[a] Yongsheng Wang,*[a] and Hui Zhao*[b]

Received Date
Accepted Date

DOI: 10.1039/xxxxxxxxxx

www.rsc.org/journalname

Due to their atomic thinness with reduced dielectric screening, two-dimensional materials can possess a stable excitonic population at room temperature. This is attractive for future excitonic devices, where excitons are used to carrier energy or information. In excitonic devices, controlling transport of the charge-neutral excitons is a key element. Here we show that exciton transport in a $MoSe_2$ monolayer semiconductor can be effectively controlled by dielectric screening. A $MoSe_2$ monolayer was partially covered by a hexagonal boron nitride flake. Photoluminescence measurements showed that the exciton energy in the covered region is about 12 meV higher than the uncovered region. Spatiotemporally resolved differential reflection measurements performed at the junction between the two regions revealed that this energy offset is sufficient to drive excitons across the junction for about 50 ps over a distance of about 200 nm. These results illustrate the feasibility of using van der Waals dielectric engineering to control exciton transport and contribute to understanding effects of dielectric environment on electronic and optical properties of two-dimensional semiconductors.

1 Introduction

Current generation of electronic devices use electrons to carrier energy or information. Their small de Broglie wavelength allows nanoscale device sizes and thus high-density integration. However, as charged particles, electrons interact strongly with their environment, leading to fast decoherence and strong inhomogeneity. Photonic devices, on the other hand, can harness the excellent coherent properties of light. However, they demand micrometer-scale dimensions and thus are challenging for high-density integration. Excitons, formed by electrons and holes, are neutral quasi-particles with a nanometer size. Thus, they can potentially combine the advantages of electrons and photons. Indeed, excitonic devices have been previously proposed and demonstrated [1,2]. However, their application has been hindered because in most semiconductors the excitons are unstable at room temperature.

The recently discovered two-dimensional (2D) semiconductors [3,4] offer a promising system for excitonic devices. Due to the enhanced Coulomb interaction, the exciton binding energies in these materials are much larger than the room-temperature thermal energy, making excitons stable at room temperature [5,6]. Excitons in 2D semiconductors also showed novel transport properties even at room temperature [7]. Hence, excitons in 2D semiconductors can be used to couple electronic and photonic systems, or even in future room-temperature excitonic devices [8]. For such applications, controlling transport of the electric-neutral excitons in 2D semiconductors is a key requirement.

Here we demonstrate an approach to control exciton transport by altering the local dielectric environment. The method is based on the fact that in 2D materials the Coulomb interaction between charged particles extends to the environment, which provides opportunities to control the electronic and optical properties of 2D materials by manipulating their surroundings [9–15]. Specifically, we control exciton transport in a $MoSe_2$ monolayer by using a hexagonal boron nitride (h-BN) top layer. We show that the h-BN layer increases the optical bandgap of $MoSe_2$, and thus creates an energy offset at the junction to drag excitons across the junction. Very recently, lateral homojunctions with controllable charge currents have been achieved by local gating [16–19], chemical doping [20], and strain engineering [21]. However, control of neutral exciton transport has been rarely demonstrated. Our results illustrate the feasibility of using dielectric engineering to control exciton transport. They also contribute to understanding effects of the dielectric environment on excitons and charge carriers in general. With industry trends beginning to move towards 3D device integration, it is likely that future applications of 2D materials will also involve multilayer structures. Thus, understanding the

[a] Key Laboratory of Luminescence and Optical Information, Ministry of Education, Institute of Optoelectronic Technology, Beijing Jiaotong University, Beijing 100044, China. E-mail: yshwang@bjtu.edu.cn

[b] Department of Physics and Astronomy, The University of Kansas, Lawrence, Kansas 66045, USA. E-mail: huizhao@ku.edu

† Electronic Supplementary Information (ESI) available: Raman spectrum of monolayer $MoSe_2$, discussion of the rigid-shift model.

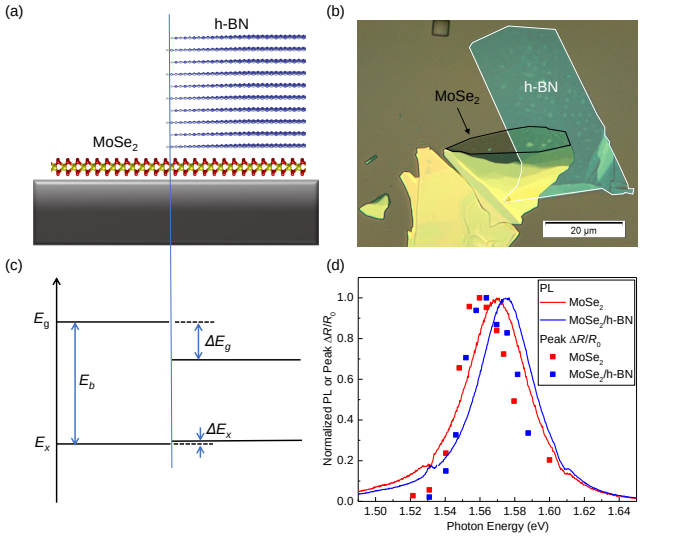

Fig. 1 (a) Schematics of sample structure. (b) Optical microscope image of one of the samples used in this study. (c) Energy diagram of the sample showing the bandgap (E_g) and exciton energy (E_x) of the uncovered (left) and covered regions of $MoSe_2$ monolayer (right) (d) Normalized photoluminescence (curves) and peak differential reflection signal (symbols) measured from the uncovered (red) and covered (blue) regions of $MoSe_2$.

effect of neighboring materials on excitons and charge carriers is important.

2 Experimental

2.1 Sample Fabrication

Figure 1(a) shows schematically the structure of the sample studied, where a monolayer $MoSe_2$ on a Si/SiO_2 substrate is partially covered by an h-BN multilayer. The sample was fabricated by mechanical exfoliation followed by a dry transfer process. First, $MoSe_2$ flakes were exfoliated from a bulk crystal to a polydimethylsiloxane (PDMS) substrate. A monolayer flake was identified according to its optical contrast, by using previously established relations between the green channel contrast and the thickness for thin layers on transparent substrates[22,23]. The monolayer flake was then transferred onto a Si/SiO_2 (90 nm) substrate and annealed at 200°C in a H_2/Ar environment for 2 hours. To further confirm its monolayer thickness, Raman spectrum was measured (see ESI) and the result is consistent with previously reported Raman spectra of monolayer $MoSe_2$[24,25]. A relatively thick h-BN flake (about 5 - 10 nm, estimated by optical contrasts[26]) was obtained by the same exfoliation procedure and was transferred on top of the $MoSe_2$ monolayer. The actual sample is shown in Figure 1(b).

Due to the screening effect of the h-BN top layer, the electronic structure of $MoSe_2$ monolayer is expected to be modified[10,27–29]. Figure 1(c) shows the transport bandgap (E_g), the optical bandgap (or exciton energy, E_x), and the exciton binding energy (E_b) of the uncovered (left) and covered (right) regions of the $MoSe_2$ monolayer, where $E_g = E_x + E_b$. Due to the screening effect of h-BN, E_g is reduced by an amount of ΔE_g. Previous studies have revealed that the screening effect on the electron-hole interaction also reduces E_b by a similar amount. As a result, the change of E_x, $\Delta E_x = \Delta E_g - \Delta E_b$, can be very small[10,27–29].

2.2 Photoluminescence Spectroscopy

In photoluminescence (PL) measurements, a 405-nm continuous-wave laser beam was focused through a microscope objective lens to a size of about 1 μm. The resulting PL emission spectra are shown in Figure 1(d) for the uncovered (red curve) and covered regions (blue curve) of $MoSe_2$, respectively. Both spectra are normalized for better comparison. In both regions, the PL is dominated by the radiative recombination of the A-excitons in $MoSe_2$[30]. The PL peak energy of the covered region is about 12 meV larger than the uncovered region. Furthermore, the PL peak of the covered region is higher by a factor of about 2.4 than that from the uncovered region. The small change of the PL energy can be attributed to the near-perfect cancellation of the changes in E_g and E_b by h-BN[10,27–29]. It is interesting to note that the sign of ΔE_x shows that the change in E_b is slightly larger than that of E_g. We note that the optical measurements performed here can only obtain ΔE_x. However, it has been reported that the change of E_g could be on the order of a fraction of 1 eV[10]. In addition, the h-BN of 5 - 10 nm is expected to be thick enough to screen the majority part of the field, producing the nearly maximum effect.

2.3 Spatially Resolved Transient Absorption Measurements

The spatiotemporally resolved differential reflection measurements were performed with a transient absorption microscope. A Ti-doped sapphire laser produces 100 fs pulses near 790 nm, with a repetition rate of 80 MHz. Part of this output was directly used as the probe pulse. The rest of it was used to pump an optical parametric oscillator to produce a 1400-nm signal output, which is frequency-doubled to 700 nm, serving as the pump pulse. The two beams are combined by a beamsplitter and are send to a microscope objective lens. The reflected probe is sent to a silicon photodiode, the output of which is measured by a lock-in amplifier referenced to a chopper that modulates the pump intensity at about 2 KHz. The spatial scan is achieved by tilting a mirror in the pump arm with a motorized mirror mount. The time scan is done by controlled by the length of the pump arm by a linear stage. Differential reflection of the probe is measured, which is defined as $\Delta R/R_0 = (R - R_0)/R_0$. Here, R and R_0 are the probe reflection with and without the presence of the pump beam, respectively. We confirm that under the experimental conditions used here, the differential reflection is approximately proportional to the injected carrier density[31,32]. Hence, its spatial and temporal variations reflects the spatiotemporal dynamics of the photocarriers.

3 Results and discussion

We first measured the peak differential reflection on each side of the junction as a function of the probe photon energy. The 1.75-eV pump pulse with a fluence of about 14 $\mu J\ cm^{-2}$ injects a peak carrier density of about $4.8\times10^{11}\ cm^{-2}$, based on an absorption coefficient of $1.37\times10^{7}\ m^{-1}$ in $MoSe_2$ for this pump energy[33]. The normalized peak differential reflection at each probe energy is shown in Figure 1(d) as the red and blue symbols for the uncov-

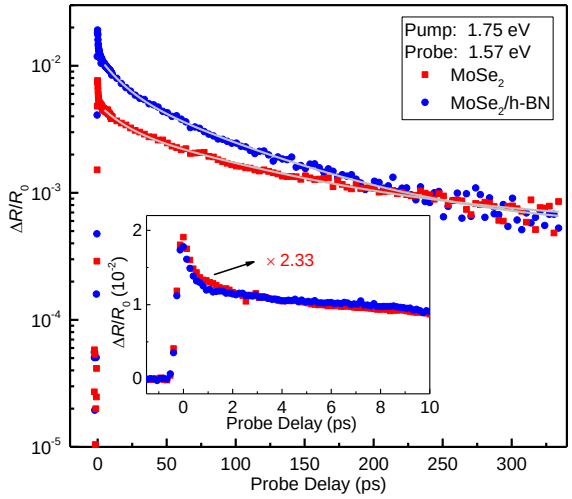

Fig. 2 Differential reflection signal of a 1.57-eV probe measured from the uncovered (red squares) and covered (blue circles) regions of the $MoSe_2$ monolayer sample, under the pump of 1.75 eV. The light-gray curves are bi-exponential fits. The inset provides a closer view of the data in early probe delays, with the data from the uncovered region scaled by a factor of 2.33.

ered and covered regions, respectively. In these measurements, the probe delay is close to zero such that the differential reflection signal is the maximum. The spectral shape of the peak differential reflection signal is similar to the PL line shape. In each region, the peak differential reflection spectrum appears to be red-shifted with respect to the PL peak. Similar to the PL results, there is a noticeable blue shift (about 10 meV) of the peak when covered with h-BN.

We next time-resolved the photocarrier dynamics by measuring the differential reflection signal as a function of probe delay. The red symbols in Figure 2 show the signal obtained with the 1.75-eV-pump and 1.57-eV-probe spots overlapped and located in the uncovered region. The same pump fluence of 14 μJ cm^{-2} was used in this measurement. The inset of Figure 2 shows the data at early probe delays. The rapid drop of the signal before 1 ps can be attributed to the formation of excitons from the injected electron-hole pairs[34,35]. The rest of the decay can be fit by a bi-exponential function with a background, $\Delta R/R_0 = A_0 + A_1 e^{-t/\tau_1} + A_2 e^{-t/\tau_2}$, as shown by the light-gray curve over the red symbols in the main panel. The two decay constants are 16 ± 2 and 114 ± 4 ps, respectively. According to previous studies, the fast time constants could reflect impact of multi-exciton processes, while the slow time constant can be attributed to the nonradiative recombination lifetime of excitons[32]. Moving the laser spots to the h-BN covered region, we studied the photocarrier dynamics in that region (blue symbols in Figure 2). The peak signal is 2.33 times higher. This factor is close to the ratio of the PL intensities of the two regions, suggesting that the difference is mainly caused by the difference in the pump powers delivered to the $MoSe_2$ layers. The two time constants are 16 ± 2 and 88 ± 4 ps, respectively. The decreased exciton lifetime when covered with h-BN could be attributed to the decreased exciton binding energy from the dielectric screening.

We now show results of spatiotemporally resolved differential

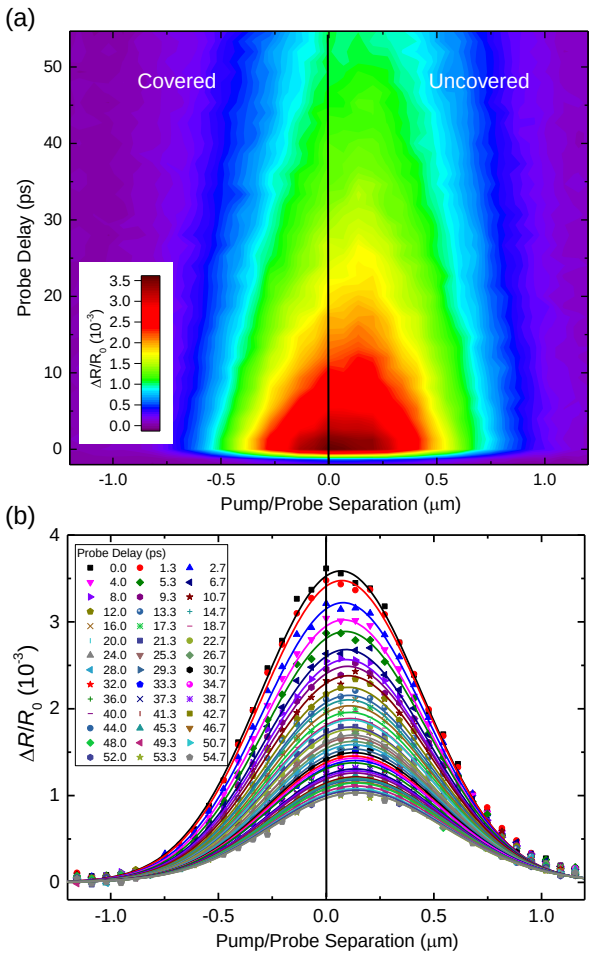

Fig. 3 (a) Spatiotemporally resolved differential reflection measurements on a junction between covered and uncovered monolayer $MoSe_2$. (b) Spatial profiles at each probe delay for the data in (a).

reflection measurements to reveal the transfer of excitons across the junction between the two regions. For these measurements, the 1.57-eV probe spot with a full-width at half maximum of about 0.6 μm is centered near the junction. A 1.68-eV pump spot of a similar size was used to inject carriers with a peak density of about 10^{12} cm^{-2}. The pump spot is scanned across the probe spot along the direction normal to the junction. At each pump position, the differential reflection signal was measured as a function of the probe delay. The results are shown in Figure 3(a). The vertical black line represents the estimated position of the junction between the covered and uncovered regions. Clearly, the peak of the measured spatial profile shifts towards the direction of uncovered region over time. This suggests that excitons formed in the covered region of the sample move across the junction into the uncovered region, driven by the energy offset. The corresponding profiles for various probe delays are plotted in Figure 3(b) as the symbols, from which the peak shift is also clearly visible.

Although the shift of the peak position is a clearly indication of the exciton transport across the junction, to quantify this process, it is necessary to deconvolute the measured profiles with the finite probe spot, since the shift is much smaller than the spot sizes used in the measurement. For this purpose, we used a rigid-shift

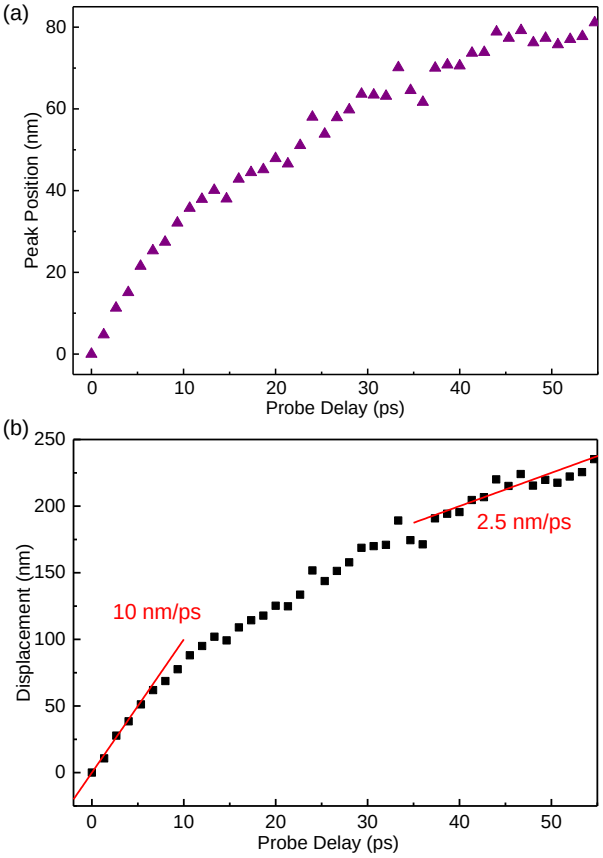

Fig. 4 (a) Peak position of the spatial profile from the model shown in Figure 3(b) as a function of probe delay. (b) The displacement of the profile deduced from the model as a function of the probe delay.

model: The exciton spatial profile at zero time was represented by the sum of two half Gaussian functions that are connect at the junction. The heights of the two halves are adjusted to match the excitation density difference of the covered and uncovered regions. For each probe delay, the half-Gaussian function of the covered side was shifted across the junction by a certain displacement. The resulted profile (that is, the sum of the two halves) is convoluted with the profile spot. The result is compared with the data and when needed, the displacement was adjusted to fit the data. Details of this procedure is given in ESI. As shown by the curves in Figure 3(b), this procedure produced profiles that are reasonably agree with the data. The peak position extracted by the model is plotted in Figure 4(a). We note that the shift of the peak position of several tens of nanometers is smaller than the laser spots of 0.6 μm. However, since the shift is determine by the fit of the entire profile, it is not limited by the laser spot. Figure 4(b) summaries the displacement of the profile deduced from the model. The exciton profile in the covered region moves with an initial speed of about 10 nm ps^{-1}, which drops to about a quarter of this value in about 30 ps. Due to the simple rigid shift model used, the speed extracted should be viewed as an order-of-magnitude estimate. Understanding the exciton transport at a quantitative level as well as the dependence on the energy offset require a more sophisticated model, which is beyond the scope of this experimental work.

4 Conclusions

In summary, we have demonstrated control of exciton transport through the dielectric screening effect. Photoluminescence and differential reflection measurements showed that covering monolayer $MoSe_2$ with h-BN increases its optical bandgap by about 12 meV. Spatiotemporally resolved differential reflection measurements performed at the junction between the uncovered and h-BN-covered regions revealed that such an offset can drive excitons from the covered to the uncovered regions, with an initial speed on the order of 10 nm ps^{-1}. These results illustrate the feasibility of using van der Waals dielectric engineering to control exciton transport and contribute to understanding effects of dielectric environment on electronic and optical properties of two-dimensional semiconductors.

5 Acknowledgement

We are grateful for the financial support of the National Key R&D Program of China (2016 YFA0202302), the National Natural Science Foundation of China (61527817, 61875236), National Science Foundation of USA (DMR-1505852), and KU Research GO project.

References

1 A. A. High, E. E. Novitskaya, L. V. Butov, M. Hanson and A. C. Gossard, *Science*, 2008, **321**, 229–231.
2 G. Grosso, J. Graves, A. T. Hammack, A. A. High, L. V. Butov, M. Hanson and A. C. Gossard, *Nat. Photo.*, 2009, **3**, 577–580.
3 E. Gibney, *Nature*, 2015, **522**, 274–276.
4 Q. H. Wang, K. Kalantar-Zadeh, A. Kis, J. N. Coleman and M. S. Strano, *Nat. Nanotechnol.*, 2012, **7**, 699–712.
5 A. Chernikov, T. C. Berkelbach, H. M. Hill, A. Rigosi, Y. L. Li, O. B. Aslan, D. R. Reichman, M. S. Hybertsen and T. F. Heinz, *Phys. Rev. Lett.*, 2014, **113**, 076802.
6 K. He, N. Kumar, L. Zhao, Z. Wang, K. F. Mak, H. Zhao and J. Shan, *Phys. Rev. Lett.*, 2014, **113**, 026803.
7 M. Kulig, J. Zipfel, P. Nagler, S. Blanter, C. Schuller, T. Korn, N. Paradiso, M. M. Glazov and A. Chernikov, *Phys. Rev. Lett.*, 2018, **120**, 207401.
8 D. Unuchek, A. Ciarrocchi, A. Avsar, K. Watanabe, T. Taniguchi and A. Kis, *Nature*, 2018, **560**, 340.
9 J. He, N. Kumar, M. Z. Bellus, H. Y. Chiu, D. He, Y. Wang and H. Zhao, *Nat. Commun.*, 2014, **5**, 5622.
10 A. Raja, A. Chaves, J. Yu, G. Arefe, H. M. Hill, A. F. Rigosi, T. C. Berkelbach, P. Nagler, C. Schuller, T. Korn, C. Nuckolls, J. Hone, L. E. Brus, T. F. Heinz, D. R. Reichman and A. Chernikov, *Nat. Commun.*, 2017, **8**, 15251.
11 S. M. Cui, H. H. Pu, S. A. Wells, Z. H. Wen, S. Mao, J. B. Chang, M. C. Hersam and J. H. Chen, *Nat. Commun.*, 2015, **6**, 8632.
12 Z. B. Song, T. Schultz, Z. J. Ding, B. Lei, C. Han, P. Amsalem, T. T. Lin, D. Z. Chi, S. L. Wong, Y. J. Zheng, M. Y. Li, L. J. Li, W. Chen, N. Koch, Y. L. Huang and A. T. S. Wee, *ACS Nano*, 2017, **11**, 9128–9135.

13 J. H. Kim, J. Lee, J. H. Kim, C. C. Hwang, C. Lee and J. Y. Park, *Appl. Phys. Lett.*, 2015, **106**, 251606.

14 Y. Li, C. Y. Xu and L. Zhen, *Appl. Phys. Lett.*, 2013, **102**, 143110.

15 P. Bolshakov, P. Zhao, A. Azcatl, P. K. Hurley, R. M. Wallace and C. D. Young, *Appl. Phys. Lett.*, 2017, **111**, 032110.

16 J. S. Ross, P. Klement, A. M. Jones, N. J. Ghimire, J. Yan, D. G. Mandrus, T. Taniguchi, K. Watanabe, K. Kitamura, W. Yao, D. H. Cobden and X. Xu, *Nat. Nanotechnol.*, 2014, **9**, 268–274.

17 A. Pospischil, M. M. Furchi and T. Mueller, *Nat. Nanotechnol.*, 2014, **9**, 257–261.

18 B. W. H. Baugher, H. O. H. Churchill, Y. Yang and P. Jarillo-Herrero, *Nat. Nanotechnol.*, 2014, **9**, 262–267.

19 Y. Katagiri, T. Nakamura, C. Ohata, S. Katsumoto and J. Haruyama, *Appl. Phys. Lett.*, 2017, **110**, 143109.

20 M. S. Choi, D. Qu, D. Lee, X. Liu, K. Watanabe, T. Taniguchi and W. J. Yoo, *ACS Nano*, 2014, **8**, 9332–9340.

21 L. Meng, Y. H. Zhang, S. Hu, X. F. Wang, C. S. Liu, Y. D. Guo, X. R. Wang and X. H. Yan, *Appl. Phys. Lett.*, 2016, **108**, 263104.

22 F. Ceballos, P. Zereshki and H. Zhao, *Phys. Rev. Mater.*, 2017, **1**, 044001.

23 M. Z. Bellus, M. Li, S. Lane, F. Ceballos, Q. Cui, X. C. Zeng and H. Zhao, *Nanoscale Horiz.*, 2016, **2**, 31–36.

24 S. Tongay, J. Zhou, C. Ataca, K. Lo, T. S. Matthews, J. B. Li, J. C. Grossman and J. Q. Wu, *Nano Lett.*, 2012, **12**, 5576–5580.

25 P. Tonndorf, R. Schmidt, P. Bottger, X. Zhang, J. Borner, A. Liebig, M. Albrecht, C. Kloc, O. Gordan, D. R. T. Zahn, S. M. de Vasconcellos and R. Bratschitsch, *Opt. Express*, 2013, **21**, 4908.

26 M. Z. Bellus, Z. Yang, P. Zereshki, J. Hao, S. P. Lau and H. Zhao, *Nanoscale Horiz.*, 2018, **4**, 236.

27 G. Gupta, S. Kallatt and K. Majumdar, *Phys. Rev. B*, 2017, **96**, 081403.

28 K. T. Winther and K. S. Thygesen, *2D Mater.*, 2017, **4**, 025059.

29 Y. S. Cho and T. C. Berkelbach, *Phys. Rev. B*, 2018, **97**, 041409.

30 Y. Li, A. Chernikov, X. Zhang, A. Rigosi, H. M. Hill, A. M. van der Zande, D. A. Chenet, E.-M. Shih, J. Hone and T. F. Heinz, *Phys. Rev. B*, 2014, **90**, 205422.

31 N. Kumar, Q. Cui, F. Ceballos, D. He, Y. Wang and H. Zhao, *Phys. Rev. B*, 2014, **89**, 125427.

32 F. Ceballos and H. Zhao, *Adv. Funct. Mater.*, 2017, **27**, 1604509.

33 H.-L. Liu, C.-C. Shen, S.-H. Su, C.-L. Hsu, M.-Y. Li and L.-J. Li, *Appl. Phys. Lett.*, 2014, **105**, 201905.

34 F. Ceballos, Q. Cui, M. Z. Bellus and H. Zhao, *Nanoscale*, 2016, **8**, 11681–11688.

35 P. Steinleitner, P. Merkl, P. Nagler, J. Mornhinweg, C. Schuller, T. Korn, A. Chernikov and R. Huber, *Nano Lett.*, 2017, **17**, 1455–1460.